Received: 26 November 2019 | Revised: 19 March 2020

DOI: 10.1002/navi.383

ORIGINAL ARTICLE

WILEY ION

Mesh topology based clock synchronization technique for pseudolite systems

Tengfei Wang[1,2] | **Zheng Yao**[1,2] | **Mingquan Lu**[1,2]

[1] Department of Electronic Engineering, Tsinghua University, Beijing, China

[2] Beijing National Research Center for Information Science and Technology, Beijing, China

Correspondence
Zheng Yao, Department of Electronic Engineering, Tsinghua University, Beijing, China.
Email: yaozheng@tsinghua.edu.cn

Funding information
National Natural Science Foundation of China, Grant/Award Number: 61771272

Abstract

Clock synchronization is critical for synchronous pseudolite systems. Wireless synchronization methods are desirable for their flexibility in system deployment, and most of them build a tree topology of time information flow based on master-slave synchronization between pseudolites. A slave pseudolite can receive signals broadcast by multiple pseudolites; however, existing methods usually utilize one signal and ignore others in which the time information could improve synchronization precision and reliability. We present a mesh topology based clock synchronization (MTCS) technique by utilizing all received signals. MTCS builds a mesh topology of time information flow, which can keep synchronization in case of link interruption or pseudolite failure. The coupling relationship of slave clocks is derived, and the influence of measurement biases is analyzed. As shown by both analysis and simulations, MTCS has better clock synchronization precision. When link interruption or pseudolite failures occur, MTCS is more robust than tree topology based methods.

KEYWORDS
clock synchronization, Kalman filter, mesh topology, pseudolite

1 | INTRODUCTION

Global Navigation Satellite Systems (GNSSs) can provide all-weather positioning, navigation, and timing services, which have been widely used in both civil and military fields over the past few decades. However, in harsh environments such as urban canyons, the availability and accuracy of GNSS are greatly affected by the lack of visible satellites. In applications such as aircraft landing, the reliability and accuracy of GNSS might be unable to meet stringent requirements.

As a solution to this issue, pseudolites are widely valued for their flexibility and high precision. Their concept and applications were explored by early researchers in order to improve the performance of GPS (Beser & Parkinson, 1982; Klein & Parkinson, 1984). Pseudolites broadcast GNSS-like signals, and compared with other positioning approaches, they are convenient to integrate with GNSS in open air environments (Cobb, 1997; Jiang, Li, & Rizos, 2015; Kiran & Bartone, 2004; Lee, Wang, Rizos, & Grejner-Brzezinska, 2004; Montillet et al., 2009).

Early pseudolites were simply transmitters that re-broadcast GNSS signals, whereas some later pseudolites can transmit and receive GNSS-like signals simultaneously. In many recent implementations, pseudolites have been stand-alone systems and are able to provide positioning services in GNSS-denied environments. A series of experiments has proved that pseudolites can provide high-precision positioning services from centimeter to decimeter level (Barnes et al., 2003; Kee et al., 2000; LeMaster, 2002; Wang, Yao, & Lu, 2019a, 2019b; Yun & Kee, 2002).

For pseudolite systems, clock synchronization precision directly affects the accuracy of measurements and has a crucial influence on positioning performance, since the coordinates of receivers are determined via the principle of time difference of arrival (TDOA). Only with high-precision clock synchronization can carrier-phase measurements be used in precise positioning (Wang, 2002).

Clock synchronization can be achieved via wired or wireless links between pseudolites. Wired synchronization has high reliability and precision and has been used in some indoor pseudolite systems. However, due to the wired links, this approach lacks flexibility and limits the system deployment, especially in outdoor applications.

Wireless synchronization is desirable for flexibility and convenience in system deployment. For pseudolites simply consisting of transmitters, wireless synchronization involves a reference station, which monitors pseudolites' signals and generates synchronization data for all clocks (Yun & Kee, 2002). For pseudolites that can receive and transmit signals simultaneously, the reference station is not necessary. For example, pseudolites that consist of self-differencing transceivers can be synchronized by two-way measuring without position information (Lee, So, Kim, & Kee, 2007; LeMaster, 2002). In the Locata system, the clock synchronization is realized by one-way measuring with the known coordinates of pseudolites (Barnes et al., 2003).

Most existing wireless methods are based on master-slave synchronization between neighboring pseudolites (Barnes et al., 2003; Lee et al., 2007; LeMaster, 2002). That is to say, they usually select a master pseudolite to provide the clock reference, with the others as slave pseudolites. Slave pseudolites visible to the master can maintain synchronization by continuously tracking the signal of the master pseudolite. Otherwise, slave pseudolites can achieve cascade synchronization by tracking the signal of a slave pseudolite that has been synchronized with the master. In such a master-slave way, clock synchronization is accomplished throughout the system, and a tree topology is built with the master pseudolite as the root.

Nevertheless, the tree topology of existing wireless methods has some disadvantages in reliability and precision. With only one-way time information flow, existing methods are fragile in case of failures. In a tree topology, there is only one synchronization path from a slave pseudolite to the master pseudolite, and any unexpected link interruption or pseudolite failure can block the synchronization of pseudolites along the path. Although such failures can be detected, it is hard to maintain or restore synchronization in a master-slave way since a slave pseudolite has only local information. Further, if the master pseudolite fails, the entire system will be out of synchronization, which is undesirable in practice.

On the other hand, the feasibility of cascade synchronization indicates that the time information useful for clock synchronization exists not only in the ranging signal of the master pseudolite, but also in the signals of synchronized slave pseudolites. Furthermore, for each slave pseudolite, most existing methods use only one signal, which is usually received from the master pseudolite, and do not utilize other signals to improve synchronization precision.

Hence, one disadvantage of the tree topology based methods is that they fail to take advantage of all signals that a pseudolite can receive, which can degrade clock synchronization performance and make the system susceptible to failures.

In this paper, we propose a mesh topology based clock synchronization (MTCS) method for pseudolite systems. Its core innovations are to use all signals that a slave pseudolite can receive and establish a mesh topology of time information flow. A local MTCS filter is established to reduce random noise for each slave pseudolite and improve the synchronization precision without additional link cost. Since clocks of slave pseudolites influence each other, a global model of MTCS is established to analyze their coupling relationship as well as the influences of measurement biases. Furthermore, it is shown that the dense topology of MTCS is beneficial for keeping all pseudolites synchronized in case of link interruptions or pseudolite failures.

The remainder of this paper is arranged as follows. First, in Section 2, the basic model is established for the clock and measurements, and the evaluation on synchronization performance is discussed. In Section 3, the local MTCS filter as well as the tracking loop is derived to reduce random noise. In Section 4, a global model of MTCS is established to analyze the coupling relationship of slave clocks and the constant differences caused by measurement biases. The advantages of MTCS in synchronization precision and performance with failures are shown. In Section 5, a series of simulations are done to verify the performance of MTCS. Finally, conclusions are drawn in Section 6.

2 | SYSTEM MODEL

In this section, a typical clock model based on state space is reviewed and then the measurement model between a pair of neighboring pseudolites is established. In addition, the evaluation on synchronization performance is discussed.

Herein, we consider a system consists of $N+1$ pseudolites labeled as $PL_0, PL_1, \ldots, PL_N$ and assume that PL_0 serves as the master pseudolite providing the clock reference for the system.

2.1 | Clock model

The clock model and performance evaluation has been widely studied. In this research, a two-state clock model is used

$$\underbrace{\begin{pmatrix} t[k] \\ f[k] \end{pmatrix}}_{\mathbf{x}[k]} = \underbrace{\begin{pmatrix} 1 & \mathrm{T_s} \\ 0 & 1 \end{pmatrix}}_{\mathbf{F}} \underbrace{\begin{pmatrix} t[k-1] \\ f[k-1] \end{pmatrix}}_{\mathbf{x}[k-1]} + \underbrace{\begin{pmatrix} w_t[k] \\ w_f[k] \end{pmatrix}}_{\mathbf{w}[k]}, \tag{1}$$

where k denotes the epoch count, $t[k]$ and $f[k]$ represent the time and frequency, $\mathrm{T_s}$ denotes the sampling interval, $w_t[k]$ and $w_f[k]$ are the noise of time and frequency, respectively (Brown & Hwang, 1997; Van Dierendonck, McGraw, & Brown, 1984).

The variance matrix $\mathbf{Q} = \mathbb{E}\{w[k]w^{\mathrm{T}}[k]\}$ characterizes the instability of the crystal oscillator. The value of $\mathbf{Q}$ can be determined as following:

$$\mathbf{Q} = \begin{pmatrix} S_t \mathrm{T_s} + \dfrac{S_f \mathrm{T_s}^3}{3} & \dfrac{S_f \mathrm{T_s}^2}{2} \\ \dfrac{S_f \mathrm{T_s}^2}{2} & S_f \mathrm{T_s} \end{pmatrix}, \tag{2}$$

where

$$S_t = 2h_0, S_f = 8\pi^2 h_{-2}, \tag{3}$$

where h_0 and h_{-2} are the coefficients of white and random walk frequency noise, respectively. Typical values are given by Brown and Hwang (Brown & Hwang, 1997).

2.2 | Measurement model

Similar to existing methods, the proposed method is based on the measurements of clock differences between a pair of neighboring pseudolites.

Suppose that there is a line-of-sight (LoS) path between PL_i and PL_j, and then the TOA measurement obtained by PL_i can be modeled as

$$\theta_{ij}[k] = t_j[k] + \tau_{ij} + e_{ij} + n_{ij}[k], \tag{4}$$

where τ_{ij} represents the propagation delay between PL_i and PL_j, e_{ij} represents the multipath error and tropospheric delays, and $n_{ij}[k] \sim \mathcal{N}(0, \sigma_{ij}^2)$ represents the measurement noise at the kth epoch.

Since all pseudolites are stationary and their coordinates can be precisely surveyed in advance, the value of τ_{ij} is assumed to be known. Then, the following observation is obtained

$$y_{ij}[k] = t_j[k] + b_{ij} + n_{ij}[k], \tag{5}$$

where b_{ij} represents the measurement bias and is assumed to be constant or change very slowly.

Time measurements are typically obtained via the code-phase estimation (Barnes et al., 2003; LeMaster, 2002). Technologies that can help to mitigate the multipath effects include multiple antennas and multi-frequency techniques (Dai, Wang, Rizos, & Han, 2002; Montillet, Bonenberg, Hancock, & Roberts, 2014). Tropospheric delays can be estimated using appropriate models (Dai et al., 2002; Wang, Wang, Sinclair, & Lee, 2005). The residual biases after using these techniques are assumed to be included in b_{ij}.

In addition, a time-hopping technique is usually used to mitigate near-far effects, and the internal system interference is ignored in this research (Borio & Odriscoll, 2014).

2.3 | Synchronization performance

Before further elaborating on the proposed method, we formalize the notations of synchronization states. **Full synchronization** means that for a period, all pseudolites share the common clock time

$$t_i[k] = t_0[k], i = 1, 2, \ldots, N, \tag{6}$$

and **frequency synchronization** means that for a period, all pseudolites share the same clock frequency

$$f_i[k] = f_0[k], i = 1, 2, \ldots, N. \tag{7}$$

This research allows constant clock differences and its main goal is to optimize the precision of frequency synchronization. In this case, the clock differences of pseudolites are constant and can be mitigated by other techniques such as two-way ranging (Lee et al., 2007; LeMaster, 2002).

Moreover, for double differential measurements widely used in precise positioning, the constant clock differences of pseudolites are eliminated and have no influence on positioning accuracy. For traditional single-point positioning, constant clock biases can have a critical influence. However, with high-precision frequency synchronization, several recent studies have achieved centimeter-level positioning accuracy, in which constant clock differences of pseudolites are absorbed in generalized carrier-phase ambiguities and resolved (Wang et al., 2019a, 2019b).

Hence, random noise is the main concern in the evaluation of synchronization performance. In the next section, a local MTCS filter will be derived to reduce random noise, and the constant clock differences caused by measurement biases will be discussed in Section 4.

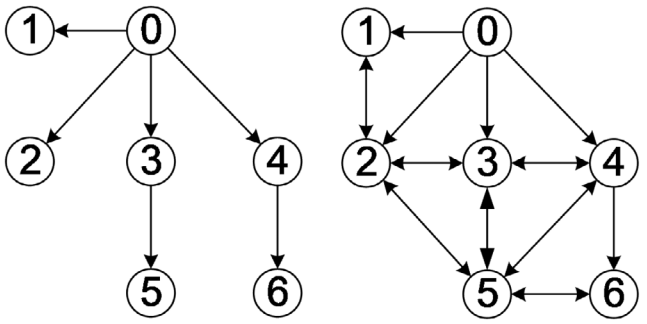

(a) Tree topology **(b)** Mesh topology

FIGURE 1 Time information flow of exisiting methods and MTCS. Each circle represents one pseudolite, and the arrows show the directions of information flow between pseudolites

3 | MESH TOPOLOGY BASED CLOCK SYNCHRONIZATION

Most existing methods are based on master-slave synchronization between pseudolites, resulting in a tree topology as shown in Figure 1a. PL_0 is the master pseudolite, and the arrow indicates the direction of time information flow. PL_1-PL_4 are directly synchronized with PL_0, whereas PL_5 and PL_6 are not visible to PL_0 and synchronized with other slave pseudolites. In such a master-slave way, clock synchronization is achieved.

As discussed in the introduction, although a pseudolite can usually receive signals from multiple neighbors, only one signal is utilized. Hence, it is reasonable to improve synchronization performance by making use of all received signals.

On the other hand, in existing methods, the tree topology is quite fragile when link interruption or pseudolite failures occur. For example, in Figure 1a, PL_5 will be influenced when PL_3 fails or the link between PL_0 and PL_3 is interrupted due to obstruction. Although slave pseudolites can detect such failures, it is difficult to quickly and correctly select another pseudolite as an alternative. More seriously, the entire system will be out of synchronization if PL_0 fails.

In MTCS, all the received signals are utilized to reduce random noise, building a mesh topology as shown in Figure 1b. When a few links or pseudolite failures occur, the synchronization will not be interrupted as long as the entire network is connected.

To improve the synchronization precision, the MTCS filter is derived based on the state space model. At the kth epoch, all observations that a slave pseudolite PL_i can obtain are denoted as $y_{i0}[k], y_{i1}[k], \dots, y_{iN}[k]$. With Equations (1) and (4), the state space model is established as

$$\mathbf{x}_0[k] = \mathbf{F}\mathbf{x}_0[k-1] + \mathbf{w}_0[k]$$

$$\underbrace{\begin{pmatrix} y_{i0}[k] \\ y_{i1}[k] \\ \vdots \\ y_{iN}[k] \end{pmatrix}}_{\mathbf{y}_i[k]} = \underbrace{\begin{pmatrix} \mathbf{h}^{\mathrm{T}} \\ \mathbf{h}^{\mathrm{T}} \\ \vdots \\ \mathbf{h}^{\mathrm{T}} \end{pmatrix}}_{\mathbf{H}} \mathbf{x}_0[k] + \underbrace{\begin{pmatrix} b_{i0} \\ b_{i1} \\ \vdots \\ b_{iN} \end{pmatrix}}_{\mathbf{b}_i} + \mathbf{e}_i[k], \tag{8}$$

where $\mathbf{h}^{\mathrm{T}} = [1\ 0]$ and

$$\mathbf{e}_i[k] = \begin{pmatrix} n_{i0}[k] \\ \mathbf{h}^{\mathrm{T}}(\mathbf{x}_1^-[k] - \mathbf{x}_0[k]) + n_{i1}[k] \\ \vdots \\ \mathbf{h}^{\mathrm{T}}(\mathbf{x}_N^-[k] - \mathbf{x}_0[k]) + n_{N1}[k] \end{pmatrix}. \tag{9}$$

If there is no LoS path between PL_i and PL_j, we have $\sigma_{ij}^2 = \infty$, and we specify $\sigma_{ii}^2 = \infty$. In addition, we assume $\mathbf{x}_j^-[k] = [t_j[k]\ \ f_j[k]]^{\mathrm{T}}$, which will be explained later. We also use a trick that $t_j[k] = t_0[k] + (t_j[k] - t_0[k])$ to introduce $\mathbf{x}_0[k]$ and obtain the expression of $\mathbf{y}_i[k]$ in Equations (8) from (5).

If we follow the traditional establishment of a Kalman filter and try to reduce the error of time synchronization, the variance matrix of $\mathbf{b}_i$ is required. However, as in the discussion in Section 2.3, the clock differences can be mitigated in a number of ways on the basis of frequency synchronization. On the other hand, some precise positioning techniques only require frequency synchronization.

Therefore, we allow constant clock differences and establish the local MTCS filter to reduce the random noise by taking $\mathbf{e}_i[k]$ as observation errors. The impact of measurement biases will be analyzed in Section 4.

Taking $\mathbf{e}_i[k]$ as observation errors, the local MTCS filter corresponding to Equation (8) is written as

$$\mathbf{x}_i^-[k] = \mathbf{F}\mathbf{x}_i^+[k-1] \tag{10}$$

$$\mathbf{P}_{ii}^-[k] = \mathbf{F}\mathbf{P}_{ii}^+[k-1]\mathbf{F}^{\mathrm{T}} + \mathbf{Q} \tag{11}$$

$$\mathbf{K}_i[k] = \mathbf{P}_{ii}^-[k]\mathbf{H}^{\mathrm{T}}(\mathbf{H}\mathbf{P}_{ii}^-[k]\mathbf{H}^{\mathrm{T}} + \mathbf{R}_i[k])^{-1} \tag{12}$$

$$\mathbf{P}_{ii}^+[k] = (\mathbf{I}_2 - \mathbf{K}_i[k]\mathbf{H})\mathbf{P}_{ii}^-[k] \tag{13}$$

$$\mathbf{x}_i^+[k] = \mathbf{x}_i^-[k] + \mathbf{K}_i[k]\big(\mathbf{y}_i[k] - \mathbf{H}\mathbf{x}_i^-[k]\big), \tag{14}$$

where $\mathbf{x}_i^-[k]$ and $\mathbf{x}_i^+[k]$ represent the *a priori* and *a posteriori* estimate, $\mathbf{P}_{ii}^-[k] = \mathbb{E}\{(\mathbf{x}_i^-[k] - \mathbf{x}_0[k])(\mathbf{x}_i^-[k] - \mathbf{x}_0[k])^{\mathrm{T}}\}$ and $\mathbf{P}_{ii}^+[k] = \mathbb{E}\{(\mathbf{x}_i^+[k] - \mathbf{x}_0[k])(\mathbf{x}_i^+[k] - \mathbf{x}_0[k])^{\mathrm{T}}\}$ are the *a priori* and *a posteriori* variance matrices, $\mathbf{K}_i$ denotes the Kalman gain, $\mathbf{I}_M$ represents the M-dim identity matrix, and $\mathbf{R}_i[k] = \mathbb{E}\{\mathbf{e}_i[k]\mathbf{e}_i^{\mathrm{T}}[k]\}$. The detailed derivation of the *a priori* and *a posteriori* covariance matrices can be found in the Appendix.

Note that $n_{i0}[k]$ is irrelevant with other observation errors in Equation (9), and $\mathbf{R}_i[k]$ can be written as

$$\mathbf{R}_i[k] = \begin{pmatrix} \sigma_{i0}^2 & \\ & \tilde{\mathbf{R}}_i[k] \end{pmatrix} = \begin{pmatrix} \sigma_{i0}^2 & & \\ & \sigma_{i1}^2 + \mathbf{h}^{\mathrm{T}}\mathbf{P}_{11}^{-}[k]\mathbf{h} \cdots & \mathbf{h}^{\mathrm{T}}\mathbf{P}_{1N}^{-}[k]\mathbf{h} \\ & \vdots \quad \ddots & \vdots \\ & \mathbf{h}^{\mathrm{T}}\mathbf{P}_{N1}^{-}[k]\mathbf{h} \cdots & \sigma_{iN}^2 + \mathbf{h}^{\mathrm{T}}\mathbf{P}_{NN}^{-}[k]\mathbf{h} \end{pmatrix}, \tag{15}$$

where $\mathbf{P}_{ij}^{-}[k] = \mathbb{E}\{(\mathbf{x}_i^{-}[k] - \mathbf{x}_0[k])(\mathbf{x}_j^{-}[k] - \mathbf{x}_0[k])^{\mathrm{T}}\}$ denotes the *a priori* covariance matrix.

Herein, for convenience of expression, it is specified that if a certain diagonal element of a matrix is ∞, the corresponding row and column in the inverse matrix are all zero.

Now, we derive the tracking loop based on the local MTCS filter. From Equation (8), it can be seen that

$$\mathbf{H} = \mathbf{1}_{N+1}\mathbf{h}^{\mathrm{T}}, \tag{16}$$

where $\mathbf{1}_M$ represents an M-dim column vector of all 1. According to the matrix inversion lemma, we have

$$\begin{aligned} &(\mathbf{H}\mathbf{P}_{ii}^{-}[k]\mathbf{H}^{\mathrm{T}} + \mathbf{R}_i[k])^{-1} \\ &= (\mathbf{1}_{N+1}\mathbf{h}^{\mathrm{T}}\mathbf{P}_{ii}^{-}[k]\mathbf{h}\mathbf{1}_{N+1}^{\mathrm{T}} + \mathbf{R}_i[k])^{-1} \\ &= \mathbf{R}_i^{-1}[k] - \frac{\mathbf{R}_i^{-1}[k]\mathbf{1}_{N+1}\mathbf{1}_{N+1}^{\mathrm{T}}\mathbf{R}_i^{-1}[k]}{\left(\mathbf{h}\mathbf{P}_{ii}^{-}[k]\mathbf{h}^{\mathrm{T}}\right)^{-1} + \mathbf{1}_{N+1}^{\mathrm{T}}\mathbf{R}_i^{-1}[k]\mathbf{1}_{N+1}}. \end{aligned} \tag{17}$$

Define a new gain matrix $\mathbf{G}_i[k]$ as

$$\mathbf{G}_i[k] = \begin{pmatrix} g_{1i}[k] \\ g_{2i}[k] \end{pmatrix} = \frac{\mathbf{P}_{ii}^{-}[k]\mathbf{h}}{(\mathbf{1}_{N+1}^{\mathrm{T}}\mathbf{R}_i^{-1}[k]\mathbf{1}_{N+1})^{-1} + \mathbf{h}^{\mathrm{T}}\mathbf{P}_{ii}^{-}[k]\mathbf{h}}. \tag{18}$$

Now substitute Equations (16)–(18) into Equation (12), and the gain matrix $\mathbf{K}_i[k]$ can be represented as

$$\begin{aligned} \mathbf{K}_i[k] &= \mathbf{P}_{ii}^{-}[k]\mathbf{h}\mathbf{1}_{N+1}^{\mathrm{T}}(\mathbf{H}\mathbf{P}_{ii}^{-}[k]\mathbf{H}^{\mathrm{T}} + \mathbf{R}_i[k])^{-1} \\ &= \frac{\mathbf{P}_{ii}^{-}[k]\mathbf{h}\mathbf{1}_{N+1}^{\mathrm{T}}\mathbf{R}_i^{-1}[k]}{1 + \mathbf{h}\mathbf{P}_{ii}^{-}[k]\mathbf{h}^{\mathrm{T}}\mathbf{1}_{N+1}^{\mathrm{T}}\mathbf{R}_i^{-1}[k]\mathbf{1}_{N+1}} \\ &= \frac{\mathbf{G}_i[k]\mathbf{1}_{N+1}^{\mathrm{T}}\mathbf{R}_i^{-1}[k]}{\mathbf{1}_{N+1}^{\mathrm{T}}\mathbf{R}_i^{-1}[k]\mathbf{1}_{N+1}^{\mathrm{T}}}. \end{aligned} \tag{19}$$

Putting Equation (19) into Equation (14) obtains

$$\mathbf{x}_i^{+}[k] = \mathbf{x}_i^{-}[k] + \mathbf{G}_i[k]\left(\hat{t}_i[k] - \mathbf{h}^{\mathrm{T}}\mathbf{x}_i^{-}[k]\right), \tag{20}$$

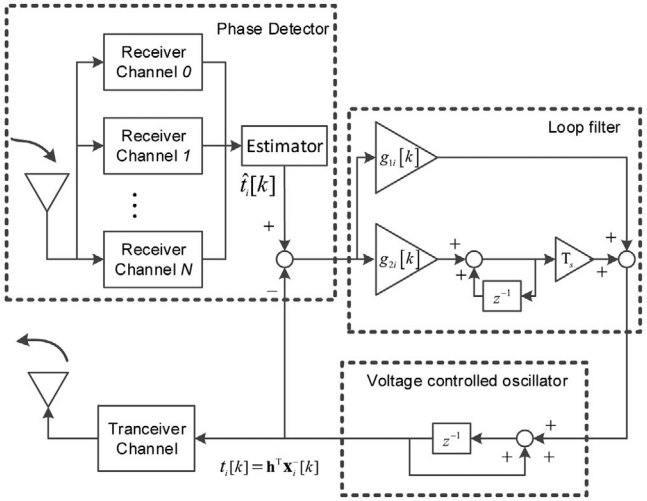

FIGURE 2 The implementation structure of the proposed local MTCS filter

where

$$\hat{t}_i[k] = \frac{\mathbf{1}_{N+1}^{\mathrm{T}}\mathbf{R}_i^{-1}[k]\mathbf{y}_i[k]}{\mathbf{1}_{N+1}^{\mathrm{T}}\mathbf{R}_i^{-1}[k]\mathbf{1}_{N+1}}. \tag{21}$$

In this way, the update equation of the *posteriori* estimate is implemented by the second-order tracking loop, while $\hat{t}_i[k]$ represents the new information from the observations.

With Equation (20), the function of the MTCS filter is easier to understand and can be implemented by a second-order loop

$$\begin{pmatrix} t_i[k+1] \\ f_i[k+1] \end{pmatrix} = \mathbf{F}\begin{pmatrix} t_i[k] \\ f_i[k] \end{pmatrix} + \mathbf{F}\mathbf{G}_i[k]\left(\hat{t}_i[k] - t_i[k]\right). \tag{22}$$

An implementation structure of the MTCS filter is shown in Figure 2. In the phase detector, multiple channels obtain time measurements from the code-phase estimation of received signals (Barnes et al., 2003; LeMaster, 2002). Then, the estimator defined by Equation (21) obtains the optimal estimate $\hat{t}_i[k]$ from these time measurements, and the local time is subtracted from it to obtain the input of the loop filter. With Equation (20), the filter in the figure is the second order, and its gain coefficients are given by Equation (18).

It can also be seen from Figure 2 that the *a priori* estimate defines the local time of a pseudolite, based on which pseudolites broadcast signals. Hence, the time information delivered by PL_i's signal is

$$t_i[k] = \mathbf{h}^{\mathrm{T}}\mathbf{x}_i^{-}[k]. \tag{23}$$

This explains why the observation equations in Equation (9) contain $\mathbf{x}_j^{-}[k]$ instead of $t_j[k]$.

With the local MTCS filter, each slave pseudolite utilizes all of its received signals and does not require additional data links.

4 | PERFORMANCE ANALYSIS

In the previous section, a local MTCS filter is derived to reduce the random noise, and an implementation structure is then derived.

In this section, a global model of MTCS is established to describe the coupling relationship of slave clocks. Then, the synchronization precision as well as the influence of measurement biases will be analyzed. In addition, the advantages of MTCS will be discussed in case of system failures.

4.1 | Coupling relationships of slave clocks

From Figure 2, it is seen that a slave pseudolite can broadcast and receive time information simultaneously, when the slave clocks are coupled in MTCS. In addition, the measurement biases will cause constant clock differences to be in steady state, and such influences will be broadcast among slave pseudolites.

As a result, it is difficult to show the coupling relationship with the local structure in Equation (20). Hence, in this subsection, we will establish a global model of MTCS to help to analyze the influences of measurement biases.

For the convenience of derivation, denote the local time and frequencies of all slave pseudolites as two vectors

$$\begin{aligned}\mathbf{t}[k] &= (t_i[k], t_2[k], \dots, t_N[k])^{\mathrm{T}}\\ \mathbf{f}[k] &= (f_1[k], f_2[k], \dots, f_N[k])^{\mathrm{T}}.\end{aligned} \tag{24}$$

With the definition above, by considering Equation (22) of all slave pseudolites together, the coupling relationships of clocks can be expressed as

$$\begin{aligned}\mathbf{t}[k+1] &= \mathbf{t}[k] + \mathrm{T_s}\mathbf{f}[k] + (\mathbf{G}_1[k] + \mathrm{T_s}\mathbf{G}_2[k])\hat{\mathbf{t}}[k]\\ \mathbf{f}[k+1] &= \mathbf{f}[k] + \mathbf{G}_2[k]\hat{\mathbf{t}}[k],\end{aligned} \tag{25}$$

where $\mathbf{G}_1[k]$ and $\mathbf{G}_2[k]$ are two diagonal matrices

$$\mathbf{G}_1[k] = \begin{pmatrix} g_{11}[k] & & \\ & \ddots & \\ & & g_{1N}[k] \end{pmatrix}, \mathbf{G}_2[k] = \begin{pmatrix} g_{21}[k] & & \\ & \ddots & \\ & & g_{2N}[k] \end{pmatrix}.$$

Herein, $\hat{\mathbf{t}}[k]$ represents the global time information, which is written as

$$\hat{\mathbf{t}}[k] = \mathbf{C}^{-1}[k][\mathbf{B}(t_0[k]\mathbf{1}_N - \mathbf{t}[k]) - \mathbf{A}[k]\mathbf{t}[k] + \mathbf{b}], \tag{26}$$

where

$$\mathbf{C}[k] = \begin{pmatrix} \mathbf{1}_{N+1}^{\mathrm{T}}\mathbf{R}_1^{-1}[k]\mathbf{1}_{N+1} & & \\ & \ddots & \\ & & \mathbf{1}_{N+1}^{\mathrm{T}}\mathbf{R}_N^{-1}[k]\mathbf{1}_{N+1} \end{pmatrix} \tag{27}$$

$$\mathbf{B} = \begin{pmatrix} \frac{1}{\sigma_{10}^2} & & \\ & \ddots & \\ & & \frac{1}{\sigma_{N0}^2} \end{pmatrix}. \tag{28}$$

Matrix $\mathbf{A}[k]$ is denoted as

$$\mathbf{A}[k] = \underbrace{\begin{pmatrix} \mathbf{1}_N^{\mathrm{T}}\tilde{\mathbf{R}}_1^{-1}[k]\mathbf{1}_N & & \\ & \ddots & \\ & & \mathbf{1}_N^{\mathrm{T}}\tilde{\mathbf{R}}_N^{-1}[k]\mathbf{1}_N \end{pmatrix}}_{\mathbf{A}_d[k]} - \underbrace{\begin{pmatrix} \mathbf{1}_N^{\mathrm{T}}\tilde{\mathbf{R}}_1^{-1}[k] \\ \vdots \\ \mathbf{1}_N^{\mathrm{T}}\tilde{\mathbf{R}}_N^{-1}[k] \end{pmatrix}}_{\mathbf{A}_1[k]}, \tag{29}$$

and the measurement biases are summarized as a vector

$$\mathbf{b} = \left(\mathbf{b}_1^{\mathrm{T}}\mathbf{R}_1^{-1}[k]\mathbf{1}_{N+1}, \dots, \mathbf{b}_N^{\mathrm{T}}\mathbf{R}_N^{-1}[k]\mathbf{1}_{N+1}\right)^{\mathrm{T}}. \tag{30}$$

It is more convenient to analyze the coupling relationship of all slave clocks based on the global model in Equation (25), which is obtained by simply putting Equation (20) together for $1 \le i \le N$. The global time information is represented by $\hat{\mathbf{t}}[k]$ in Equation (26) and consists of three parts; matrix $\mathbf{A}[k]$ characterizes the coupling relationship of the clocks of slave pseudolites; matrix $\mathbf{B}$ describes the one-way information propagation from the master pseudolite; and the measurement biases $\mathbf{b}$ will result in constant clock differences.

In Equation (26), the term $\mathbf{A}[k]\mathbf{t}[k]$ describes the information exchange of slave pseudolites with each other. It is not difficult to prove that the matrix $\mathbf{A}[k]$ satisfy that

$$\mathbf{A}[k]\mathbf{1}_N = \mathbf{0}. \tag{31}$$

This means that when the clock time of slave pseudolite are different, $\mathbf{A}[k]\mathbf{t}[k]$ in Equation (26) will drive them to be consistent.

On the other hand, if the slave clocks are not synchronized with the master clock, the term $\mathbf{B}(t_0[k]\mathbf{1}_N - \mathbf{t}[k])$ will be nonzero and drive them to achieve time synchronization.

If PL_i is not visible to PL_0, its synchronization relies on the information of neighboring slave pseudolites. Under the influences of these two terms, the system can achieve clock synchronization.

In MTCS, a certain measurement bias will affect multiple pseudolites. The vector $\mathbf{b}$ describes the influence of measurement biases on the global time information, which will result in constant clock differences.

In fact, the tree topology is a special case of the mesh topology. If there is no information exchange between slave pseudolites, we have $\mathbf{A}[k] = \mathbf{O}$ and $\mathbf{B} = \mathbf{I}_N$. In this case, MTCS will degenerate into a tree topology based method.

4.2 | Constant clock differences

In this subsection, the steady state is derived to analyze the influence of $\mathbf{b}$. For tree topology based methods and MTCS, measurement biases can cause constant clock differences, so that only frequency synchronization can be achieved.

Let $\mathbf{f}[k+1] = \mathbf{f}[k]$ and from Equation (25), it can be obtained that

$$\mathbf{A}[k]\mathbf{t}[k] + \mathbf{B}\mathbf{t}[k] - \mathbf{B}t_0[k]\mathbf{1}_N = \mathbf{b}. \tag{32}$$

With Equation (31), we have $\mathbf{A}[k]t_0\mathbf{1}_N = \mathbf{0}$ and

$$\mathbf{A}[k]\mathbf{t}[k] = \mathbf{A}[k]\mathbf{t}[k] - \mathbf{A}[k]t_0\mathbf{1}_N. \tag{33}$$

Putting this into Equation (32), it is obtained that

$$(\mathbf{A}[k] + \mathbf{B})\delta\mathbf{t}[k] = -\mathbf{b}, \tag{34}$$

where the vector $\delta\mathbf{t}[k]$ denotes the clock differences between the master and slave pseudolites

$$\delta\mathbf{t}[k] = t_0[k]\mathbf{1}_N - \mathbf{t}[k]. \tag{35}$$

Therefore, in the steady state, the constant clock differences are written as a vector

$$\delta\mathbf{t}_\infty = -(\mathbf{A}[\infty] + \mathbf{B})^{-1}\mathbf{b}. \tag{36}$$

In MTCS, clock differences are represented as the linear combination of measurement biases in Equation (36).

Similar analysis can be performed on tree topology based methods. For example, if all slave pseudolites are visible to the master pseudolite, we have $\mathbf{A}[k] = \mathbf{O}$, and $\mathbf{C}^{-1}\mathbf{B}[k] = \mathbf{I}_N$. As a result, the clock differences can be represented as

$$\delta\mathbf{t}_\infty = -(b_{10}, b_{20}, \dots, b_{N0})^{\mathrm{T}}. \tag{37}$$

If a slave pseudolite is synchronized in a cascade fashion, the clock differences will be the sum of biases along the links. For instance, in Figure 1a, the constant clock differences of PL_5 will be $-(b_{30} + b_{53})$.

Nevertheless, due to the lack of a reasonable model of measurement biases, it is difficult to compare the performance of different topologies.

4.3 | Synchronization precision

In this subsection, it will be proved by mathematical induction that MTCS has smaller *a priori* and *a posteriori* estimation errors than tree topology based methods. Similar to the traditional analysis of filter design, the following discussion is mainly focused on the random noise.

First, denote the *a priori* and *a posteriori* variance matrix respectively as $\tilde{\mathbf{P}}_{ii}^{-}[k]$ and $\tilde{\mathbf{P}}_{ii}^{+}[k]$ for tree topology based methods, respectively. Assume that for $k = m-1$, there have been $\mathbf{P}_{ii}^{+}[m-1] \preceq \tilde{\mathbf{P}}_{ii}^{+}[m-1]$. The notation $\mathbf{X} \preceq \mathbf{Y}$ denotes that matrix $\mathbf{Y} - \mathbf{X}$ is semi-positive.

Then, for $k = m$, it can be obtained that

$$\begin{aligned}\mathbf{P}_{ii}^{-}[m] - \tilde{\mathbf{P}}_{ii}^{-}[m] =& \mathbf{F}\mathbf{P}_{ii}^{+}[m-1]\mathbf{F}^{\mathrm{T}} - \mathbf{F}\tilde{\mathbf{P}}_{ii}^{+}[m-1]\mathbf{F}^{\mathrm{T}} \\ =& \mathbf{F}\left(\mathbf{P}_{ii}^{+}[m-1] - \tilde{\mathbf{P}}_{ii}^{+}[m-1]\right)\mathbf{F}^{\mathrm{T}} \\ \preceq& \mathbf{O},\end{aligned} \tag{38}$$

which yields $\mathbf{P}_{ii}^{-}[m] \preceq \tilde{\mathbf{P}}_{ii}^{-}[m]$.

On the other hand, according to the information form of the Kalman filter, we have the following two equations

$$(\mathbf{P}_{ii}^{+}[m])^{-1} = (\mathbf{P}_{ii}^{-}[m])^{-1} + \mathbf{h}\mathbf{1}_{N+1}^{\mathrm{T}}\mathbf{R}_i^{-1}[k]\mathbf{1}_{N+1}\mathbf{h}^{\mathrm{T}} \tag{39}$$

$$(\tilde{\mathbf{P}}_{ii}^{+}[m])^{-1} = (\tilde{\mathbf{P}}_{ii}^{-}[m])^{-1} + \mathbf{h}\tilde{\sigma}_i^{-2}\mathbf{h}^{\mathrm{T}}, \tag{40}$$

where $\tilde{\sigma}_i^2$ denotes the variance of observation errors for tree topology based methods. With additional observations in MTCS, it can be said that

$$\mathbf{1}_{N+1}^{\mathrm{T}}\mathbf{R}_i^{-1}[k]\mathbf{1}_{N+1} - \tilde{\sigma}_i^{-2} \geq 0. \tag{41}$$

Then, it can be obtained that

$$\begin{aligned}&(\mathbf{P}_{ii}^{+}[m])^{-1} - (\tilde{\mathbf{P}}_{ii}^{+}[m])^{-1} \\ =&(\mathbf{P}_{ii}^{-}[m])^{-1} - (\tilde{\mathbf{P}}_{ii}^{-}[m])^{-1} + \mathbf{h}(\mathbf{1}_{N+1}^{\mathrm{T}}\mathbf{R}_i^{-1}[k]\mathbf{1}_{N+1} - \tilde{\sigma}_i^{-2})\mathbf{h}^{\mathrm{T}} \\ \succeq&(\mathbf{P}_{ii}^{-}[m])^{-1} - (\tilde{\mathbf{P}}_{ii}^{-}[m])^{-1} \\ \succeq&\mathbf{O},\end{aligned} \tag{42}$$

which yields $\mathbf{P}_{ii}^{+}[m] \preceq \tilde{\mathbf{P}}_{ii}^{+}[m]$.

Furthermore, for $k = 1$, the preset of the variance matrix depends only on *a priori* assumptions, which should be the same for MTCS and tree topology based methods. In other words, it is assumed that $\mathbf{P}_{ii}^{+}[0] = \tilde{\mathbf{P}}_{ii}^{+}[0]$. Then, it can be said that $\mathbf{P}_{ii}^{-}[1] = \tilde{\mathbf{P}}_{ii}^{-}[1]$.

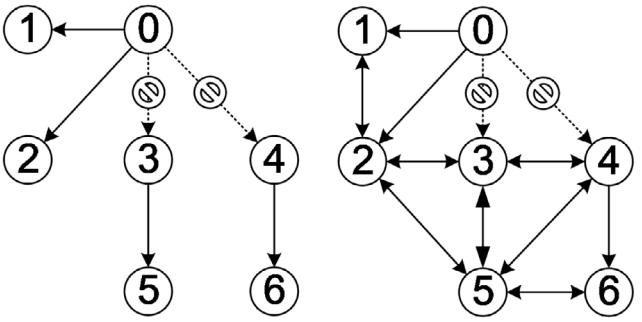

(a) Tree topology with failures **(b)** Mesh topology with failures

FIGURE 3 Examples of clock synchronization topology. The arrows show information flow, whereas PL_3 and PL_4 are not visible to PL_0 now

Based on the two results above, it can be proved that $\mathbf{P}_{ii}^{-}[k] \preceq \tilde{\mathbf{P}}_{ii}^{-}[k]$ and $\mathbf{P}_{ii}^{+}[k] \preceq \tilde{\mathbf{P}}_{ii}^{+}[k]$. According to the properties of semi-positive matrices, MTCS has smaller variance in *a priori* and *a posteriori* estimation errors and shows advantages in synchronization precision.

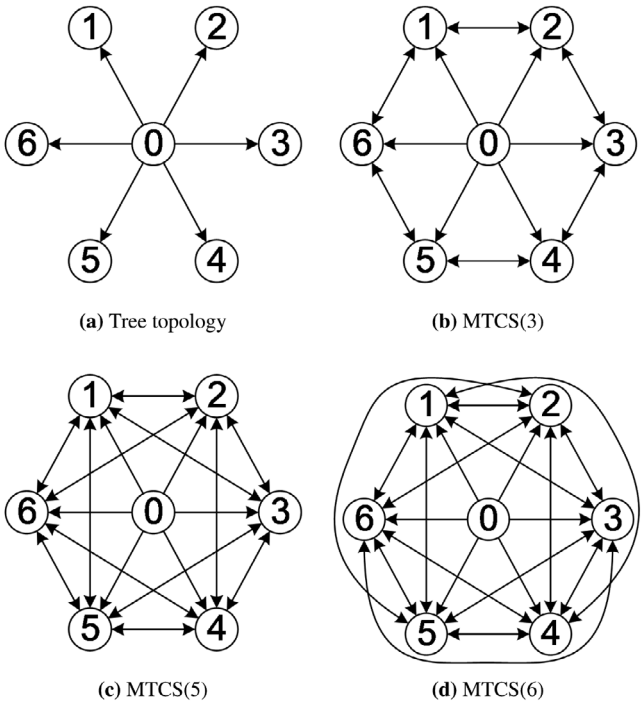

(a) Tree topology **(b)** MTCS(3)

(c) MTCS(5) **(d)** MTCS(6)

FIGURE 4 Four topologies used in the simulations

4.4 | Link interruptions and pseudolite failures

It is assumed that a slave pseudolite can detect the failures of its neighboring pseudolites or links. For tree topology based methods, when failures occur unexpectedly, a slave pseudolite might choose another neighbor to maintain synchronization, but with local information alone, it is possible to rebuild an incorrect topology.

As shown in Figure 3a, if PL_3 and PL_4 are not visible to PL_0 due to link interruptions, they might be synchronized with each other. As a result, the system is divided into two parts, and this is obviously a wrong topology for clock synchronization.

When the master pseudolite fails, the situation may be even worse. It will be difficult for pseudolites to restore synchronization based on data messages, since they have been out of synchronization.

However, in MTCS, with additional links involved in synchronization, the frequency synchronization will still be maintained if the network is connected. As shown in Figure 3b, PL_3-PL_6 can keep clock synchronization via information from PL_2, even though they have no knowledge of topology changes. Matrices $\mathbf{A}[k]$ and $\mathbf{B}$ will change according to the new information flow topology.

When pseudolite failures occur, it is not difficult to draw similar conclusions. A special situation is that the master pseudolite fails or all its links fail. In this case, $\mathbf{B}$ will be a zero matrix, and in Equation (26), $\hat{\mathbf{t}}[k]$ will only depend on the clock difference between slave pseudolites. It will result in a distributed synchronization, which is another topic (Giridhar & Kumar, 2006; Mallada & Tang, 2011).

It is not difficult to see that a dense network is desirable for dealing with such failures, and this is an advantage of MTCS over tree topology based methods.

In the future, a topic to be studied is how to choose the master pseudolite when considering the failure problem.

5 | SIMULATIONS

In this section, the performance of MTCS will be verified by numerical simulations involving seven pseudolites. PL_0 is the master pseudolite and visible to all others, and four different topologies are shown in Figure 4.

The tree topology is shown in Figure 4a, while MTCS(n) refers to that each slave pseudolite is visible to n other pseudolites as shown in Figures 4b, 4c, and 4d. It can be seen that from MTCS(3) to MTCS(6), the links in the topology are strictly increased, and for MTCS(6), all pseudolites are visible to each other.

The typical values of clock parameters in Equation (3) are set as $h_0 = 2 \times 10^{-19}$ and $h_{-2} = 2 \times 10^{-20}$ for a low-quality temperature compensating crystal oscillator (TCXO) (Brown & Hwang, 1997). All simulations are performed with MATLAB.

TABLE 1 The initial error of slave pseudolites. All values are scaled by 1×10^{-8}

	1	2	3	4	5	6
$\delta t_i[k]$ (s)	2.40	3.55	0.45	1.14	−3.30	5.18
$\delta f_i[k]$ (Hz)	−6.29	−4.18	4.89	−5.99	−1.86	−7.07

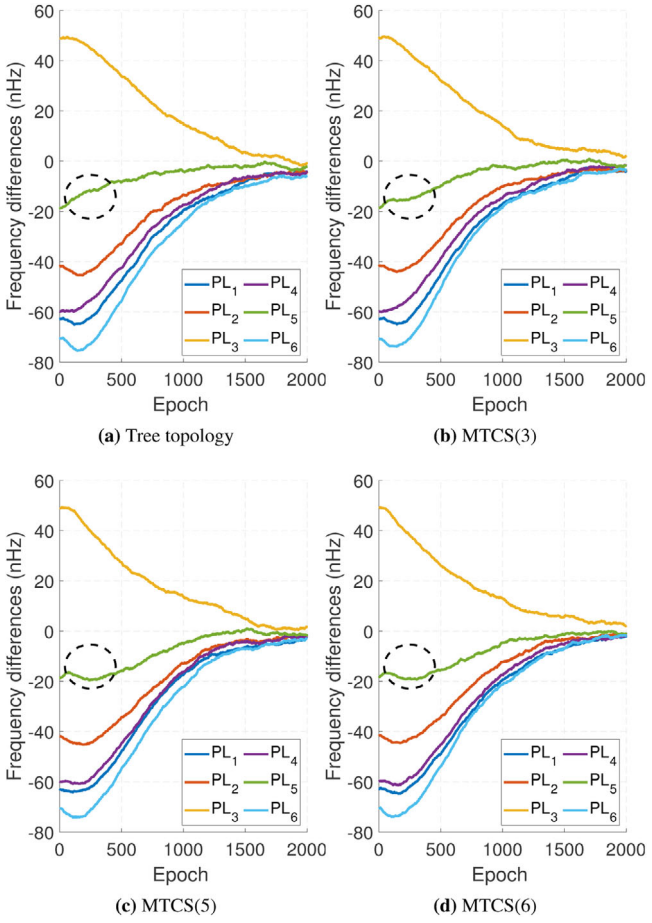

FIGURE 5 Comparison of frequency differences in transient processes without failures [Color figure can be viewed in the online issue, which is available at wileyonlinelibrary.com and www.ion.org]

5.1 | Transient process

In this subsection, the transient process of MTCS is compared with that of tree topology based methods. There is no system failure in the simulation. With 10.23 MHz code rate, 1 ms loop update interval, 10% duty cycle, and 60 dB·Hz C/N_0, the standard deviation of code-phase estimation is about 0.01 code chip, and in this case, the time measurement noise is set as 1 ns (Cheong, 2012).

The initial states of slave pseudolites can be found in Table 1. The transient processes with the four topologies are shown in Figure 5 and in the subfigures where a curve represents the frequency difference of specific pseudolite. The variation of clock differences in the transient processes is shown in Figure 6.

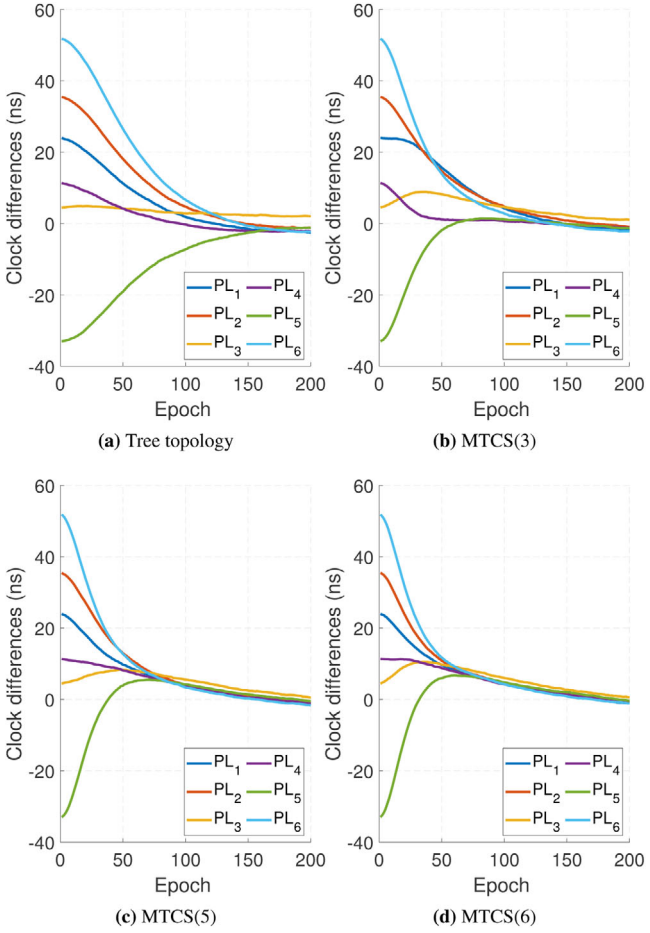

FIGURE 6 Comparison of clock differences in transient processes without failures [Color figure can be viewed in the online issue, which is available at wileyonlinelibrary.com and www.ion.org]

It can be seen from Figure 5 that in the four topologies, all slave pseudolites can achieve frequency synchronization, and their frequency differences gradually reach near zero. However, the transient processes with the four topologies are different. For example, in the initial stage, the frequency of PL_5 in the tree topology is significantly different from those in mesh topologies, which is indicated by dotted circles in the subfigures.

In fact, such differences of the transient processes in the four topologies can be seen more clearly in Figure 6. With the tree topology in Figure 4a, the convergence process of each slave clock is irrelevant with others, whereas in MTCS, the slave clocks reach approximately the same state first and then gradually converge.

This is consistent with the analysis in Section 4.1. Due to the information exchanges between pseudolites, which are represented by $\mathbf{A}[k]$ in Equation (26), the slave clocks are coupled and driven by $\mathbf{A}[k]\mathbf{t}[k]$ to arrive at a common state.

This phenomena can be clearly seen in Figures 6c and 6d in the first 70 epochs, but is less obvious in Figure 6b.

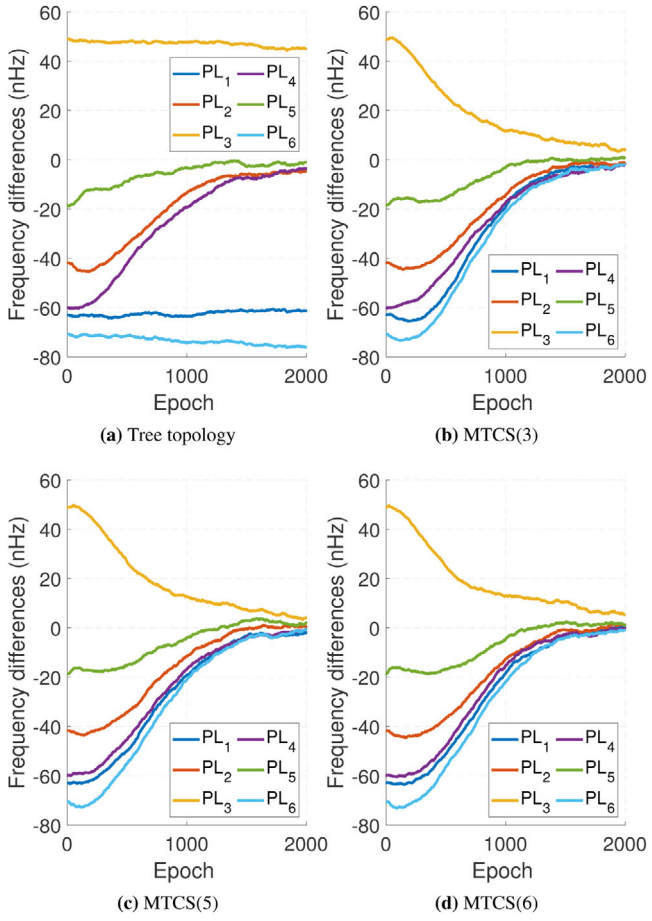

FIGURE 7 Comparison of frequency differences in transient processes with link failures [Color figure can be viewed in the online issue, which is available at wileyonlinelibrary.com and www.ion.org]

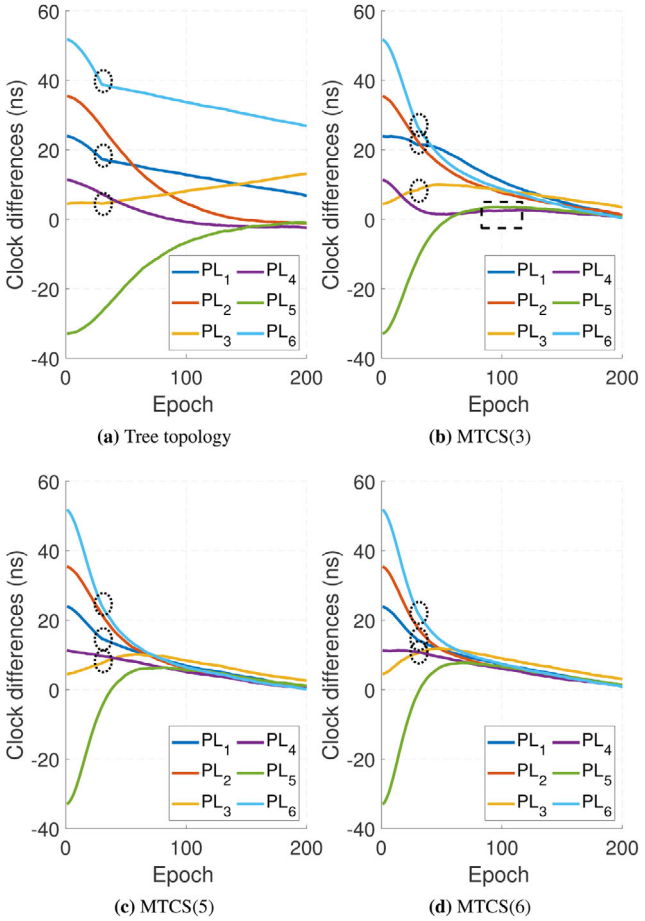

FIGURE 8 Comparison of clock differences in transient processes with link failures [Color figure can be viewed in the online issue, which is available at wileyonlinelibrary.com and www.ion.org]

This is because the topology of MTCS(3) is relatively sparse and characterizes fewer information exchanges between slave pseudolites.

On the other hand, the time information from PL_0, which is represented by $\mathbf{B}(t_0[k]\mathbf{1}_N - \mathbf{t}[k])$, makes all slave pseudolites achieve synchronization. As a result, the slave clocks converge in a similar process after the 100th epoch in Figures 6b, 6c, and 6d.

5.2 | Behaviors with system failures

In this subsection, the behaviors of MTCS with system failures are investigated. The four topologies in Figure 4 are used, but the communication links $PL_1 - PL_0$, $PL_3 - PL_0$, and $PL_6 - PL_0$ are interrupted at the 30th epoch. Other parameters are the same as those in the previous simulation.

The frequency and time differences in transient processes are shown in Figures 7 and 8, respectively, and the link interruption points are indicated by dotted circles in Figure 8.

It can be seen from Figure 7a that in the tree topology, PL_1, PL_3, and PL_6 can not be synchronized and their frequency differences stay near a fixed value, while other slave pseudolites can achieve synchronization. This shows that the tree topology is very vulnerable to such failures. Nevertheless, as shown in Figure 7, all pseudolites can be synchronized in MTCS. In this regard, the mesh topology shows its robustness advantages.

By analyzing the change of topology, it is not difficult to conclude that in the tree topology, other slave pseudolites are not affected by link interruptions. This can also be seen by comparing Figures 6a and 8a.

However, in MTCS, such link interruptions cause some changes of transient processes due to the information exchange between slave pseudolites. For example, as shown by Figure 6b, the clock differences of PL_4 and PL_5 in MTCS(3) reach almost zero at the 100th epoch in the previous simulation, but with the link interruptions in this simulation, they are positive as indicated by the dotted rectangular in Figure 8b.

In addition, it can be seen that, compared to Figure 8b, the curve changes at the interruption points are less

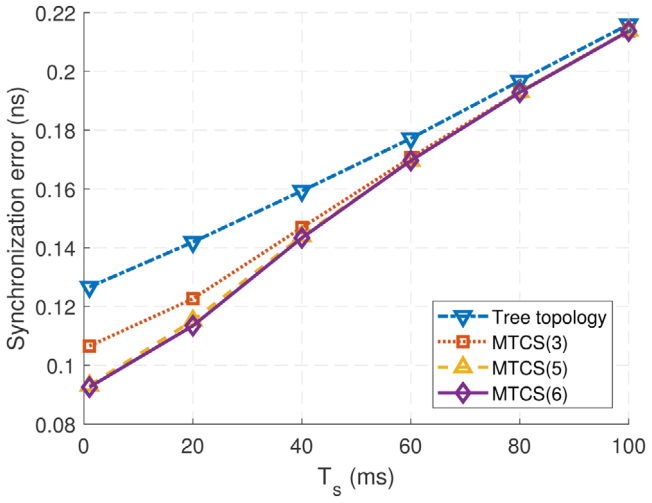

FIGURE 9 Comparison of synchronization precision with different topologies and loop update intervals [Color figure can be viewed in the online issue, which is available at wileyonlinelibrary.com and www.ion.org]

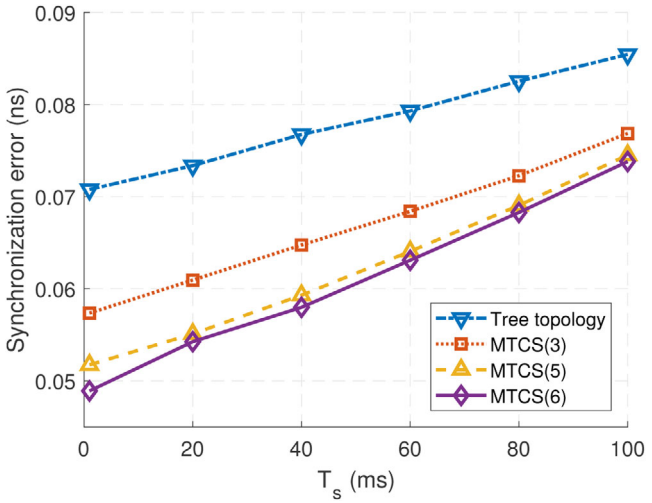

FIGURE 10 Comparison of synchronization precision with a TCXO model of better quality [Color figure can be viewed in the online issue, which is available at wileyonlinelibrary.com and www.ion.org]

significant in Figures 8c and 8d. This is because MTCS(5) and MTCS(6) have denser topologies than MTCS(3) and are less affected.

5.3 | Synchronization precision

The synchronization precision of MTCS is verified in this simulation. The loop update interval T_s varies from 1 ms to 100 ms. With $T_s = 1$ ms, the standard deviation of measurement noise is set as 1 ns. If T_s is increased to 10 ms, the noise level will be reduced to $1/\sqrt{10}$ ns, and so on. The four topologies in Figure 4 are still used for this simulation.

In each case with specific T_s, 100 Monte Carlo trials are performed. The synchronization precision is evaluated by the standard deviation of $t_0[k], t_1[k], \ldots, t_N[k]$. For each trial, the results in 500 epochs under steady state are averaged.

The simulation results are illustrated in Figure 9. It is shown that MTCS has better synchronization precision than tree topology based methods. The precision is improved with the increase in the number of links among pseudolites. In the four topologies, MTCS(6) achieves the best performance while MTCS(5) is quite close to it.

In addition, Figure 10 illustrates the simulation results with a TCXO model of better quality. The clock parameters in Equation (3) are set as $h_0 = 2 \times 10^{-20}$ and $h_{-2} = 2 \times 10^{-22}$, and in this case, similar conclusions on the advantages of MTCS can be drawn as shown in Figure 9.

On the other hand, it can be seen that the advantage of MTCS gradually decreases as the loop update interval T_s increases. With a larger T_s, the measurement noise is weakened; however, the instability of oscillators will have more significant influences. In this case, all slave pseudolites have worse synchronization precision, and the time information provided by them is less useful. As a result, the increase in the number of links between slave pseudolites is less crucial and the advantages of MTCS decrease.

This phenomenon is more obvious in Figure 9, since oscillators of poor quality will also degrade the time information provided by slave pseudolites. Nevertheless, it can be seen that in Figure 9, when $T_s \leq 50$ ms, MTCS has a significant advantage. In fact, a rapid loop update rate is always desirable, and a interval of tens of milliseconds is too long in practice.

6 | CONCLUSIONS

We present a new clock synchronization technique named MTCS that is based on a mesh topology for pseudolite systems. The analysis shows that each pseudolite broadcasts its *a priori* estimate of the system time, and MTCS makes better use of received signals to improve the synchronization precision. The global model of MTCS is established, and then the coupling effects of slave clocks are analyzed.

The performance of MTCS is verified by both analysis and numerical simulations. MTCS shows advantages in synchronization precision, especially with dense links and a rapid loop update rate. Another important advantage is that when link interruptions or pseudolite failures occur, MTCS is more likely to keep the entire system in synchronization.

In future research, how to choose a master pseudolite in a specific network, which can affect the synchronization precision and behaviors with system failures, is a valuable topic. In addition, we are planning to conduct real-world experiments to further verify and improve the robustness of MTCS in challenging environments.

ACKNOWLEDGMENT

This work was supported by the National Natural Science Foundation of China (NSFC) under Grant 61771272.

ORCID

Tengfei Wang https://orcid.org/0000-0001-7301-1200
Zheng Yao https://orcid.org/0000-0002-7657-644X

REFERENCES

Barnes, J., Rizos, C., Wang, J., Small, D., Voigt, G., & Gambale, N. (2003). Locata: A new positioning technology for high precision indoor and outdoor positioning. In *Proceedings of the 16th International Technical Meeting of the Satellite Division of The Institute of Navigation (ION GPS/GNSS 2003)*, pp. 1119–1128. Retrieved from https://www.ion.org/publications/abstract.cfm?articleID=5291

Beser, J., & Parkinson, B. W. (1982). The application of NAVSTAR differential GPS in the civilian community. *NAVIGATION*, *29*(2), 107–136. https://doi.org/10.1002/j.2161-4296.1982.tb00795.x

Borio, D., & Odriscoll, C. (2014). Design of a general pseudolite pulsing scheme. *IEEE Transactions on Aerospace and Electronic Systems*, *50*(1), 2–16. https://doi.org/10.1109/TAES.2013.110277

Brown, R. G., & Hwang, P. Y. C. (1997). *Introduction to random signals and applied Kalman filtering: With MATLAB exercises and solutions*. New York: Wiley.

Cheong, J. W. (2012). *Signal processing and collective detection for Locata positioning system* (PhD dissertation). University of New South Wales.

Cobb, H. S. (1997). *GPS pseudolites: Theory, design, and applications* (PhD dissertation). Stanford University.

Dai, L., Wang, J., Rizos, C., & Han, S. (2002). Pseudo-satellite applications in deformation monitoring. *GPS Solutions*, *5*(3), 80–87. https://doi.org/10.1007/PL00012902

Giridhar, A., & Kumar, P. R. (2006). Distributed clock synchronization over wireless networks: Algorithms and analysis. In *Proceedings of the 45th IEEE Conference on Decision and Control*, pp. 4915–4920. https://doi.org/10.1109/CDC.2006.377325

Jiang, W., Li, Y., & Rizos, C. (2015). Locata-based precise point positioning for kinematic maritime applications. *GPS Solutions*, *19*(1), 117–128. https://doi.org/10.1007/s10291-014-0373-9

Kee, C., Jun, H., Yun, D., Kim, B., Kim, Y., Parkinson, B. W., … Lee, J. T. (2000). Development of indoor navigation system using asynchronous pseudolites. In *Proceedings of the 13th International Technical Meeting of the Satellite Division of The Institute of Navigation (ION GPS 2000)*, pp. 1038–1045. Retrieved from https://www.ion.org/publications/abstract.cfm?articleID=1504

Kiran, S., & Bartone, C. G. (2004). Flight-test results of an integrated wideband-only airport pseudolite for the category II/III local area augmentation system. *IEEE Transactions on Aerospace and Electronic Systems*, *40*(2), 734–741. https://doi.org/10.1109/TAES.2004.1310018

Klein, D., & Parkinson, B. W. (1984). The use of pseudo-satellites for improving GPS performance. *NAVIGATION*, *31*(4), 303–315. https://doi.org/10.1002/j.2161-4296.1984.tb00881.x

Lee, H. K., Wang, J., Rizos, C., & Grejner-Brzezinska, D. (2004). Analyzing the impact of integrating pseudolite observables into a GPS/INS system. *Journal of Surveying Engineering*, *130*(2), 95–103. https://doi.org/10.1061/(ASCE)0733-9453(2004)130:2(95)

Lee, T., So, H., Kim, K., & Kee, C. (2007). Smart pseudolites array system using two-way pseudolites. In *Proceedings of the 20th International Technical Meeting of the Satellite Division of The Institute of Navigation (ION GNSS 2007)*, pp. 1477–1483. Retrieved from https://www.ion.org/publications/abstract.cfm?articleID=7351

LeMaster, E. A. (2002). *Self-calibrating pseudolite arrays: Theory and experiment* (PhD dissertation). Stanford University.

Mallada, E., & Tang, A. (2011). Distributed clock synchronization: Joint frequency and phase consensus. In *50th IEEE Conference on Decision and Control and European Control Conference*, pp. 6742–6747. https://doi.org/10.1109/CDC.2011.6161231

Montillet, J.-P., Bonenberg, L. K., Hancock, C. M., & Roberts, G. W. (2014). On the improvements of the single point positioning accuracy with Locata technology. *GPS Solutions*, *18*(2), 273–282. https://doi.org/10.1007/s10291-013-0328-6

Montillet, J.-P., Roberts, G. W., Hancock, C., Meng, X., Ogundipe, O., & Barnes, J. (2009). Deploying a Locata network to enable precise positioning in urban canyons. *Journal of Geodesy*, *83*(2), 91–103. https://doi.org/10.1007/s00190-008-0236-7

Vandierendonck, A. J., McGraw, J. B., & Brown, R. G. (1984). Relationship between Allan variances and Kalman Filter parameters. In *Proceedings of the 16th Annual Precise Time and Time Interval (PTTI) Applications and Planning Meeting*, pp. 273–293. Retrieved from https://www.ion.org/publications/abstract.cfm?articleID=16168

Wang, J. (2002). Pseudolite applications in positioning and navigation: Progress and problems. *Positioning*, *1*(03), 48–56. https://doi.org/10.5081/jgps.1.1.48

Wang, J. J., Wang, J., Sinclair, D., Watts, L., Lee, H. K. (2005). Tropospheric delay estimation for pseudolite positioning. *Journal of Global Positioning Systems*, *4*(1–2), 106–112. https://doi.org/10.5081/jgps.4.1.106

Wang, T., Yao, Z., & Lu, M. (2019). Combined difference square observation-based ambiguity determination for ground-based positioning system. *Journal of Geodesy*, *93*(10), 1867–1880. https://doi.org/10.1007/s00190-019-01288-0

Wang, T., Yao, Z., & Lu, M. (2019). On-the-fly ambiguity resolution involving only carrier phase measurements for stand-alone ground-based positioning systems. *GPS Solutions*, *23*(2), 36. https://doi.org/10.1007/s10291-019-0825-3

Yun, D., & Kee, C. (2002). Centimeter accuracy stand-alone indoor navigation system by synchronized pseudolite constellation. In *Proceedings of the 15th International Technical Meeting of the Satellite Division of The Institute of Navigation (ION GPS 2002)*, pp. 213–225. Retrieved from https://www.ion.org/publications/abstract.cfm?articleID=2019

How to cite this article: Wang T, Yao Z, Lu M. Mesh topology based clock synchronization technique for pseudolite systems. *NAVIGATION*. 2020;67:619–631. https://doi.org/10.1002/navi.383

APPENDIX: SUPPLEMENTARY DERIVATION OF THE LOCAL MTCS FILTER

First, denote the a priori covariance matrix $\mathbf{P}_{ij}^{-}[k]$ and a posteriori covariance matrix $\mathbf{P}_{ij}^{+}[k]$ as

$$\mathbf{P}_{ij}^{-}[k] = \mathbb{E}\left\{(\mathbf{x}_i^{-}[k] - \mathbf{x}_0[k])(\mathbf{x}_j^{-}[k] - \mathbf{x}_0[k])^{\mathrm{T}}\right\} \tag{A1}$$

$$\mathbf{P}_{ij}^{+}[k] = \mathbb{E}\left\{(\mathbf{x}_i^{+}[k] - \mathbf{x}_0[k])(\mathbf{x}_j^{+}[k] - \mathbf{x}_0[k])^{\mathrm{T}}\right\}. \tag{A2}$$

From the analysis in Section 2.3, the influences of biases and noise should be discussed separately. Herein, the following derivation is focused on the random noise, while the measurement biases are ignored. In fact, we can assume all the measurement biases and subtract them from the equations.

First, with Equation (20), $\mathbf{x}_i^{+}[k] - \mathbf{x}_0[k]$ can be rewritten as

$$\begin{aligned}
&\mathbf{x}_i^{+}[k] - \mathbf{x}_0[k] \\
&= \mathbf{x}_i^{-}[k] + \mathbf{G}_i[k]\left(\frac{\mathbf{1}_{N+1}^{\mathrm{T}}\mathbf{R}_i^{-1}[k]\mathbf{y}_i[k]}{\mathbf{1}_{N+1}^{\mathrm{T}}\mathbf{R}_i^{-1}[k]\mathbf{1}_{N+1}} - \mathbf{h}^{\mathrm{T}}\mathbf{x}_i^{-}[k]\right) - \mathbf{x}_0[k] \\
&= (\mathbf{I}_2 - \mathbf{G}_i[k]\mathbf{h}^{\mathrm{T}})(\mathbf{x}_i^{-}[k] - \mathbf{x}_0[k]) \\
&\quad + \frac{\mathbf{G}_i[k]\mathbf{1}_{N+1}^{\mathrm{T}}\mathbf{R}_i^{-1}[k]}{\mathbf{1}_{N+1}^{\mathrm{T}}\mathbf{R}_i^{-1}[k]\mathbf{1}_{N+1}}\left(\mathbf{y}_i[k] - \mathbf{1}_{N+1}\mathbf{h}^{\mathrm{T}}\mathbf{x}_i^{-}[k]\right).
\end{aligned} \tag{A3}$$

Define $\bar{\mathbf{P}}_j[k]$ as

$$\bar{\mathbf{P}}_j[k] = \mathbb{E}\{(\mathbf{y}_i[k] - \mathbf{h}^{\mathrm{T}}\mathbf{x}_i[k]\mathbf{1}_{N+1})(\mathbf{x}_j^{+}[k] - \mathbf{x}_0[k])^{\mathrm{T}}\}. \tag{A4}$$

It can be said that the measurement noise is independent on the *a priori* estimate, and we have

$$\bar{\mathbf{P}}_j[k] = \left(\mathbf{0}_2, \mathbf{P}_{j1}^{-}[k]\mathbf{h}, \ldots, \mathbf{P}_{jN}^{-}[k]\mathbf{h}\right)^{\mathrm{T}}. \tag{A5}$$

Then, with Equations (A3)–(A5), Equation (A2) can be rewritten as

$$\begin{aligned}
\mathbf{P}_{ij}^{+}[k] &= (\mathbf{I}_2 - \mathbf{G}_i[k]\mathbf{h}^{\mathrm{T}})\mathbf{P}_{ij}^{-}[k](\mathbf{I}_2 - \mathbf{G}_j[k]\mathbf{h}^{\mathrm{T}})^{\mathrm{T}} \\
&\quad + \frac{\mathbf{G}_i[k]\mathbf{1}_{N+1}^{\mathrm{T}}\mathbf{R}_i^{-1}[k]}{\mathbf{1}_{N+1}^{\mathrm{T}}\mathbf{R}_i^{-1}[k]\mathbf{1}_{N+1}}\bar{\mathbf{P}}_j[k](\mathbf{I}_2 - \mathbf{G}_j[k]\mathbf{h}^{\mathrm{T}})^{\mathrm{T}} \\
&\quad + (\mathbf{I}_2 - \mathbf{G}_i[k]\mathbf{h}^{\mathrm{T}})\bar{\mathbf{P}}_i^{\mathrm{T}}[k]\left(\frac{\mathbf{G}_j[k]\mathbf{1}_{N+1}^{\mathrm{T}}\mathbf{R}_j^{-1}[k]}{\mathbf{1}_{N+1}^{\mathrm{T}}\mathbf{R}_j^{-1}[k]\mathbf{1}_{N+1}}\right)^{\mathrm{T}} \\
&\quad + \frac{\mathbf{G}_i[k]\mathbf{1}_{N+1}^{\mathrm{T}}\mathbf{R}_i^{-1}[k]}{\mathbf{1}_{N+1}^{\mathrm{T}}\mathbf{R}_i^{-1}[k]\mathbf{1}_{N+1}}\bar{\mathbf{P}}[k]\left(\frac{\mathbf{G}_j[k]\mathbf{1}_{N+1}^{\mathrm{T}}\mathbf{R}_j^{-1}[k]}{\mathbf{1}_{N+1}^{\mathrm{T}}\mathbf{R}_j^{-1}[k]\mathbf{1}_{N+1}}\right)^{\mathrm{T}},
\end{aligned} \tag{A6}$$

where

$$\bar{\mathbf{P}}[k] = \begin{pmatrix} 0 & & \\ & \mathbf{h}^{\mathrm{T}}\mathbf{P}_{11}^{-}[k]\mathbf{h} & \cdots & \mathbf{h}^{\mathrm{T}}\mathbf{P}_{1N}^{-}[k]\mathbf{h} \\ & \vdots & \ddots & \vdots \\ & \mathbf{h}^{\mathrm{T}}\mathbf{P}_{N1}^{-}[k]\mathbf{h} & \cdots & \mathbf{h}^{\mathrm{T}}\mathbf{P}_{NN}^{-}[k]\mathbf{h} \end{pmatrix}. \tag{A7}$$

With Equation (A6) and $\mathbf{P}_{ij}^{-}[k] = \mathbf{F}\mathbf{P}_{ij}^{+}[k]\mathbf{F}^{\mathrm{T}} + \mathbf{Q}$, the iterative computation of $\mathbf{P}_{ij}^{-}[k]$ and $\mathbf{P}_{ij}^{+}[k]$ can be carried out.